Letter

Gate control, *g* factors, and spin-orbit energy of *p*-type GaSb nanowire quantum dot devices

Sven Dorsch,[1,*] In-Pyo Yeo,[1] Sebastian Lehmann,[1] Kimberly Dick,[1,2] Claes Thelander,[1] and Adam Burke[1,†]
[1]*Solid State Physics and NanoLund, Lund University, Box 118, SE-221 00 Lund, Sweden*
[2]*Center for Analysis and Synthesis, Lund University, Box 118, SE-221 00 Lund, Sweden*

(Received 6 April 2021; accepted 17 June 2021; published 30 June 2021; corrected 5 December 2022)

Proposals for quantum information applications are frequently based on the coherent manipulation of spins confined to quantum dots. For these applications, *p*-type III-V material systems promise a reduction of the hyperfine interaction while maintaining large *g* factors and strong spin-orbit interaction. In this Letter, we study bottom-gated device architectures to realize single and serial multiquantum dot systems in Schottky-contacted *p*-type GaSb nanowires. We find that the effect of potentials applied to gate electrodes on the nanowire is highly localized to the immediate vicinity of the gate electrode only, which prevents the formation of double quantum dots with commonly used device architectures. We further study the transport properties of a single quantum dot induced by bottom gating and find large gate-voltage dependent variations of the g^* factors up to 8.1 ± 0.2 as well as spin-orbit energies between 110 and 230 μeV.

DOI: 10.1103/PhysRevB.103.L241411

A key challenge for spintronic and quantum electronic applications is achieving long coherence and spin lifetimes [1]. Here, *p*-type materials can be beneficial in comparison to more conventional *n*-type systems [2]. In the valence band, the *p*-orbital symmetry efficiently reduces the hyperfine interaction of free holes through a suppression of the contact term [2–5].

Consequently, interest in *p*-type quantum dot (QD) devices, where the coherent manipulation of spins confined to the QD enables qubit operation [6], is growing fast and systems based on InGaAs [4], Ge [7], Si [8], or ambipolar InSb [5,9] are widely regarded as promising candidates. Another, hitherto less investigated candidate is GaSb, which due to its high hole mobility and the expected strong spin-orbit interaction in III-V semiconductors offers interesting material properties [10–12]. Hole transport in GaSb QD devices has so far only been studied in GaSb/InAsSb core-shell [13] and plain GaSb nanowires, where metallic contacts at low temperatures form Schottky barriers, allowing the formation of a QD between closely spaced electrodes [14].

Schottky barrier defined QDs are fabrication limited by the smallest achievable spacing between the contacts and the QD dimensions, and tunnel rates vary depending on the gate voltage and applied bias. Smaller QD structures, however, are beneficial as they allow easier access to quantum confinement effects in the electronic structure [14]. Consequently, an important step toward the realization of GaSb nanowire based spintronic devices is the development of device architectures allowing the formation and characterization of small QDs. For the more common nanowire material InAs, the development of local bottom gates [15] and, later, epitaxially defined InP-InAs-InP [16,17] as well as WZ-ZB-WZ polytype structures [18,19] has enabled small, tunable, and flexible high-quality QD and serial double quantum dot (DQD) devices, which are now widely used for various transport studies. For GaSb nanowires, epitaxially defined QD structures are not yet experimentally available and the design of flexible, local gate architectures is challenging for Schottky-contacted nanowires. In this Letter, we investigate to what extent control can be achieved in *p*-type GaSb:Zn nanowires by studying the transport properties of bottom-gate defined single and multiple QDs.

Arrays of of gate electrodes were fabricated on top of a back-gated Si/SiO_2 substrate and covered by a layer of HfO_2. Zinc-doped zinc blende GaAs-GaSb:Zn nanowires were deposited on top of the gate arrays and the GaSb segment was contacted by Ni/Au Schottky contacts (source and drain). Further details of the device characterization are given in the Supplemental Material (SM) [20]. For device geometry A, shown in Fig. 1(a), we use five underlying gates (g1–g5 with applied voltages V_{1-5}) with the purpose of forming a DQD. Here, g1 and g5 are located below the Schottky contacts with the aim to allow control over tunnel couplings to the contacts. Gates g2 and g4 are designed to act as plunger gates to a left (L) and right (R) QD, while g3 induces a barrier between the QDs.

Figure 1(c) shows a characteristic charge stability diagram of the device as a function of V_2 and V_4, while V_3 is held constant at -2.9 V. We find finite bias triangles, arranged along horizontal and vertical symmetry axes (dashed red lines) with additional diagonal features (enclosed by white dashed lines). This behavior is comparable to results obtained on a serial triple quantum dot (TQD) [21] and we explain this by the additional formation of a middle (M) QD atop g3, resulting in the measurement configuration indicated in red in Fig. 1(b). To verify TQD formation, we next measure the charge stability diagram as a function of V_2 and V_3 with $V_{1,4,5} = -3$ V.

*sven.dorsch@ftf.lth.se
†adam.burke@ftf.lth.se

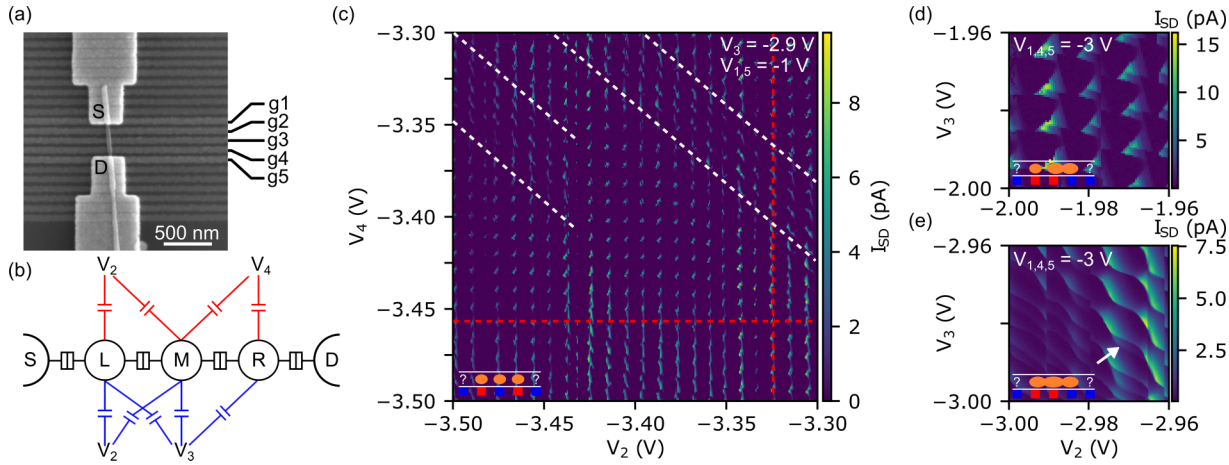

FIG. 1. (a) Scanning electron microscope image of device A, a Schottky-contacted GaSb nanowire on five gate stripes g1–g5. (b) Measurement configurations for (c) indicated in red and for (d),(e) indicated in blue. (c) Charge stability diagram as a function of V_2 and V_3 at $V_{SD} = 1$ mV. Pattern repetition axes are indicated. (d),(e) Charge stability diagram at $V_{SD} = 3$ mV as a function of V_2 and V_3 in a (d) weak-coupling and (e) strong-coupling regime between the left and middle QD. $V_{BG} = -10$ V for all measurements in Fig. 1.

In this configuration, sketched in blue in Fig. 1(b), we then expect to be able to control the interdot coupling between the left and middle QD by tuning the extent of the conductive islands within the nanowire. Indeed, for sufficiently low negative gate voltages $V_{2,3}$, we find behavior matching that of a weakly coupled DQD in Fig. 1(d). By decreasing the voltages $V_{2,3}$, shown in Fig. 1(e), the charge stability diagram transitions resemble that of a strongly coupled DQD. We note that additional cells within Fig. 1(e) (see, for example, white arrow) again indicate TQD formation.

We find transport across the device to only be possible if sufficiently negative voltages are applied to g2, g3, and g4 to form three QDs. For more positive voltages V_3, where no middle QD is formed, transport remains blocked which prevents the formation of a DQD. This, in combination with the formation of independently addressable QDs located on top of neighboring gates, indicates that gate action on the nanowire occurs only very localized by either inducing or suppressing the formation of conductive islands within the nanowire. Gaps in the gate array, for enhancement-mode nanowires, then always act as barriers. As a possible explanation for this unconventional gate response, we suggest surface trap states which efficiently screen the nanowire core from potential variations in the environment. We find comparable results in different device geometries where the gates access the nanowire from the side, indicating a cause seemingly independent of the gate design (see SM [20]). The highly localized gate action stands in contrast to other common III-V enhancement-mode nanowire systems such as thin InAs [22,23] and InSb [5,9], but also Ge/Si core-shell nanowires [24] where comparable bottom-, top-, and side-gate architectures enable the formation of DQDs.

Next, we study the effect of gates located directly under the Schottky contacts as well as the properties of QDs induced by local bottom gating in the simplified single-QD device B shown in Fig. 2(a). Here we reduce the number of bottom gates (g1–g3), where g1 and g3 are located below the Schottky contacts and g2 is designed to act as the plunger gate and to induce a short QD in the enclosed nanowire segment.

The resulting charge stability diagram is shown in Fig. 2(b). The data here are plotted as a function of the plunger gate voltage V_2, with all other gates grounded. For large negative voltages, $V_2 < -1.35$ V, the charge stability diagram resembles that of a clean QD with clear diamond-shaped Coulomb blockade regions. In contrast, for less negative V_2, additional overlaying patterns are observed and the Coulomb blockade regions are less well defined for lower occupancies. This is conceptually comparable to results obtained on *p*-type Si nanowires and are explained by a valence band roughness leading to multi-QD formation for low occupancies [25]. This effect is indicated by the insets of Fig. 2(b) and is expected to become less prominent and eventually vanish for decreased QD dimensions [25].

To study the effect of a voltage applied to g1 and g3, we next measure the charge stability diagram of the device as a function of V_1 and V_2 and find results closely following the previously described gate functionality. For sufficiently positive V_1, the nanowire segment atop g1 remains nonconductive and the resulting charge stability diagram in Fig. 2(c) shows Coulomb oscillations on the QD induced by g2, with a small cross coupling to g1. In contrast, if V_1 is chosen more negative, a second conductive island is formed atop g1. In the resulting charge stability diagram [Fig. 2(d)], this manifests as steps in the Coulomb oscillations—an indicator for Coulomb coupled QDs [26–28] where changes in occupancy of the left QD are marked by dashed white lines. Additionally, at the location of each step, finite bias triangles indicative of a DQD are observed [29]. We find the resulting system, sketched in Fig. 2(e) with all transport channels indicated, to be a hybrid between a serial and purely Coulomb coupled double quantum dot. Here, only the center QD is coupled to both contacts, while holes traveling through the left QD have to pass the middle QD to contribute to the detected current.

We next apply a positive back gate voltage $V_{BG} = 4$ V, $V_{1,3} = 1.5$ V and a sufficiently negative V_2 to ensure the formation of exclusively one QD. The charge stability diagram for the lowest occupancies where the valence band edge roughness has no further visible impact on the electronic

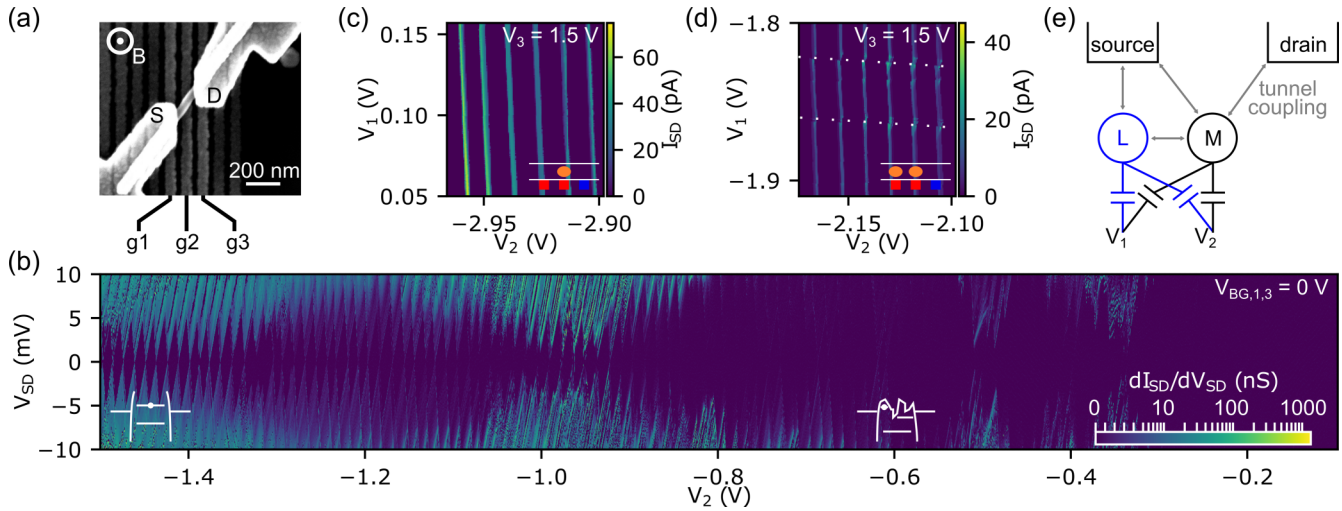

FIG. 2. (a) Scanning electron microscope image of device B, a Schottky-contacted GaSb nanowire on three gate stripes g1–g3. (b) Single-QD charge stability diagram at $V_{BG} = 0$ V and $V_{1,3} = 0$ V. Insets indicate the impact of the valence band edge. (c),(d) Charge stability diagram at $V_{SD} = 1$ mV, $V_{BG} = 0$ V as a function of V_1 and V_2 in a configuration where only (c) g2 or (d) g1 and g2 induce conductive islands in the nanowire. Insets indicate active gates (red) and QD formation. (e) Device configuration in (d).

structure is shown in Fig. 3(a) and we estimate a hole occupancy of $p \approx 25$.

To obtain information about effective g^* factors of the QD, we perform magnetotransport spectroscopy on cutline i in Fig. 3(a). The magnetic field is applied perpendicular to the nanowire, as illustrated in Fig. 2(a). Figure 3(b) shows the differential conductance along cutline i as a function of the magnetic field, where Zeeman splitting of the ground state is observed. We note that the upper branch consists of a double conductance peak, which could be the result of a nearly degenerate state at $B = 0$ T or a singlet and triplet state interacting at low magnetic fields below our resolution limit. The distance between data points on the upper and lower branches (purple and red markers) in Fig. 3(b) follows a linear slope [see Fig. 3(c)], and in either of the cases closely represents the difference in energy between states of opposite spin. A fit (solid red line) with the standard expression for Zeeman splitting, $\Delta E_z = |g^*|\mu_B B$ where μ_B is the Bohr magneton, yields $|g^*| = 2.4 \pm 0.1$. This result corresponds well to the findings in GaSb/InAsSb core-shell nanowires in a hole transport regime [13].

Magnetotransport spectroscopy measurements along cutlines near each of the crossings depicted in Fig. 3(a) were analyzed and, where Zeeman splitting is resolved, g^* factors are extracted. The resulting values found for ground- and excited-state splitting are plotted against the effective occupation number in Fig. 3(d). For an effective occupancy of 3, the observed splittings are too small to clearly resolve and $|g^*| < 0.2$ can be estimated. Overall, our data show a spread in g^* factors from almost vanishing up to $|g^*| = 8.1 \pm 0.2$ [see Fig. 4(d)], with no clear trend between successive hole occupancies.

For p-type nanowires, theory predicts large variations in g^* factors between different orbital states [30–32]; however, that does not describe the absence of coinciding results between successive occupancies. We explain the observed variations within orbital states by the required plunger gate voltage difference between different occupancies. Variations of V_2 influence the dimensions of the conductive island within the nanowire and thus alter the wave functions, leading to differences in the observed g^* factors.

An additional contribution to the g^*-factor variation is illustrated in Figs. 4(a) and 4(b), where dI_{SD}/dV_{SD} along the cutlines ii and iii is plotted as a function of the magnetic field. In both measurements, Zeeman splitting of the ground state and an excited state is observed and branches of opposite spin interact via the spin-orbit interaction, leading to an avoided crossing. While in Fig. 4(b) the twofold spin degeneracy is obvious, only the state increasing in energy within the first-excited orbital is clearly resolved in the data in Fig. 4(a). We directly extract the spacings between the ground and first-excited orbital $\Delta\epsilon_{0,1} = 1.2$ meV and $\Delta\epsilon_{0,1} = 0.5$ meV at $B = 0$ T as well as the magnitude of the avoided crossing $2\Delta_{SO} = 460$ μeV and $2\Delta_{SO} = 225$ μeV from Figs. 4(a) and 4(b), respectively. Here, based on the assumption that states remain energetically pinned by the strong coupling between the gate electrode and the QD upon variation of V_{SD}, only a factor of two between the magnitude of the avoided crossing and the spin-orbit energy Δ_{SO} is considered.

To obtain g_n^* factor estimates for the ground ($n = 0$) and first-excited ($n = 1$) orbital from Figs. 4(a) and 4(b), we normalize the data to the energy of the ground state (state with the highest energy available for transport in the valence band) and compare the result to simple calculations in Figs. 4(c) and 4(d). We thus describe the nondegenerate spin states by $E_m = \pm\frac{1}{2}|g_n^*|\mu_B B - \Delta\epsilon_{0,n} - \frac{1}{2}|g_0^*|\mu_B B$ (gray dashed lines), where the last addend normalizes the energies with respect to the ground state and $\Delta\epsilon_{0,n}$ is the energetic spacing of orbital n containing state m to the highest available orbital. For states m, m' in different orbitals and of different spin polarity, we further modify the energies by

$$E_{m,m'}^{SO} = \frac{E_m + E_{m'}}{2} \pm \frac{1}{2}\sqrt{(E_m - E_{m'})^2 + (2\Delta_{SO})^2} \quad (1)$$

to account for the spin-orbit interaction induced level repulsion [33,34].

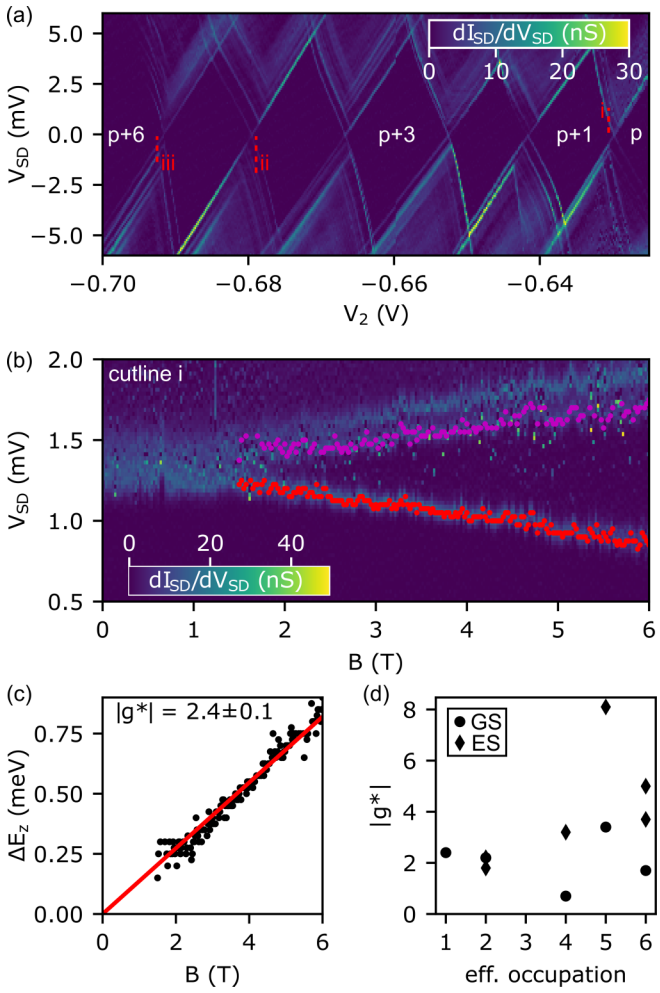

FIG. 3. (a) Lowest six clean crossings in the charge stability diagram measured at $V_{BG} = 4$ V and $V_{1,3} = 1.5$ V. (b) Differential conductance along cutline i, labeled in (a) as a function of the magnetic field. Ground-state Zeeman splitting is observed and conductance peaks corresponding to states with opposite spins are detected (red/magenta dots). (c) Fit to the Zeeman splitting ΔE_z extracted from (b). (d) $|g^*|$ for various ground-state (GS) and excited-state (ES) orbitals plotted against the effective occupation number of the QD, $p = 0$.

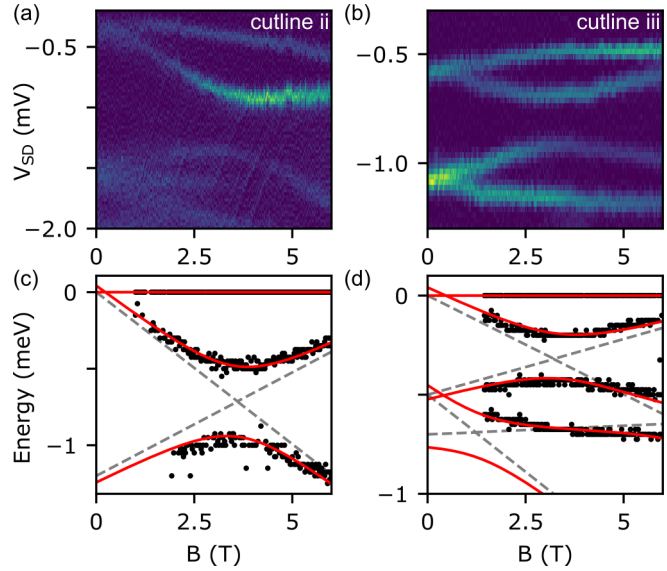

FIG. 4. (a),(b) Differential conductance along cutline ii and iii, respectively, in Fig. 3(a) as a function of the magnetic field. (c),(d) Comparison and fit of data points extracted from (a) and (b), respectively, to calculated states with (solid red line) and without (gray dashed lines) level repulsion. All energies are normalized to the energetically highest ground state available for transport in the valence band.

By fitting Eq. (1) (red lines) to the experimental data, we obtain $|g_0^*| = 3.4 \pm 0.2$ and $|g_1^*| = 8.1 \pm 0.2$ as well as $|g_0^*| = 1.7 \pm 0.2$ and $|g_1^*| = 3.7 \pm 0.2$ from Figs. 4(c) and 4(d), respectively. While this is sufficient to reproduce the data in Fig. 4(c), we note that the Zeeman split branches of the first-excited states in Fig. 4(d) appear pinched. To reproduce this shape, an additional state E_5 is considered in Fig. 4(d), which is further discussed in the SM [20].

Finally, it is important to address the zero B-field Zeeman splitting for the calculations (solid red lines) presented in Figs. 4(c) and 4(d), where a twofold spin degeneracy of all states is expected. This zero-field splitting is a result of the approximative nature of Eq. (1), which only yields accurate results for $\Delta_{SO} \ll \Delta E_z$ [33]. Thus, the extracted $|g^*|$ values are to be considered reasonable estimates. Nevertheless, a comparison of the calculations including and excluding (solid red and dashed gray lines) spin-orbit interaction in Figs. 4(c) and 4(d) clearly illustrates that a fit for g^* factors, as shown in Fig. 3(c), even in a low B-field regime, underestimates the g^* factor if avoided crossings occur. While this is taken into account in measurements where avoided crossings were obvious, those cases are not always clear within the experimental data. Consequently, the $|g^*|$ values in Fig. 3(d) should be considered as lower bounds.

In conclusion, we demonstrated the formation of serial multi- and single-QDs in enhancement-mode Schottky-contacted GaSb:Zn nanowires. Our measurements show that bottom gates can be used to form single and multiple QDs. However, we find that gates only act on the nanowire in their direct vicinity and can induce conductive islands, while gaps in gate arrays result in barrier formation. This renders common gating approaches inept for the formation of controlled serial double quantum dots. As a solution, we propose device designs based on stacked gate arrays or a combination of bottom and side, or top, gates. Further variations of the dopant concentration, nanowire diameter, or surface treatment may also lead to improved gating behavior.

Through magnetotransport spectroscopy and analyzing the observed avoided crossings, we estimate g^* factors of up to 8.1 ± 0.2 and a spin-orbit energy Δ_{SO} reaching 230 μeV. Our findings for Δ_{SO} are comparable to the results for electrons in III-V nanowire systems with effective g^* factors reaching those commonly observed in InAs [9,34–37]. A direct comparison of the properties of GaSb nanowires with other p-type nanowire systems reveals g^* factors matching or slightly exceeding those found for InSb [5], Ge-hut [7], Si [38], and Si-Ge core-shell [39] nanowires, but Δ_{SO} is up to an order

of magnitude lower compared to selected Ge based systems [7,40,41].

For spin qubits, strong spin-orbit interaction introduces a trade-off as, on one hand, it allows for fast, electric-field induced spin manipulation, but, on the other hand, also enhances dephasing though phonons and charge noise [42]. For III-V nanowire systems, a strong anisotropy of the spin-orbit interaction strength with a link between gate-induced electric fields and the orientation of the spin-orbit field has been reported [9,22]. This could allow for ideal qubit operation conditions for GaSb, where the spin-orbit interaction is selectively tuned. The next steps toward characterizing GaSb nanowire quantum devices will thus be to study the g^* factor and Δ_{SO} anisotropy, as well as to form a pure DQD and probe the various mechanisms affecting the hole spin relaxation time.

The authors thank T. Mörstedt and H. Kindlund for contributions in the early stages of the project, M. Leijnse and A. Jönsson for helpful discussions, and acknowledge funding by the Swedish Research Council (VR) (Project No. 2015-00619), the Marie Skłodowska Curie Actions, Cofund, Project No. INCA 600398, the Crafoord Foundation, and NanoLund. Device fabrication was carried out in the Lund Nano Lab (LNL).

[1] I. Žutić, J. Fabian, and S. D. Sarma, Spintronics: Fundamentals and applications, Rev. Mod. Phys. **76**, 323 (2004).

[2] D. Brunner, B. D. Gerardot, P. A. Dalgarno, G. Wüst, K. Karrai, N. G. Stoltz, P. M. Petroff, and R. J. Warburton, A coherent single-hole spin in a semiconductor, Science **325**, 70 (2009).

[3] M. H. Kolodrubetz and J. R. Petta, Coherent holes in a semiconductor quantum dot, Science **325**, 42 (2009).

[4] J. H. Prechtel, A. V. Kuhlmann, J. Houel, A. Ludwig, S. R. Valentin, A. D. Wieck, and R. J. Warburton, Decoupling a hole spin qubit from the nuclear spins, Nat. Mater. **15**, 981 (2016).

[5] V. Pribiag, S. Nadj-Perge, S. Frolov, J. Van Den Berg, I. Van Weperen, S. Plissard, E. P. A. M. Bakkers, and L. P. Kouwenhoven, Electrical control of single hole spins in nanowire quantum dots, Nat. Nanotechnol. **8**, 170 (2013).

[6] D. Loss and D. P. DiVincenzo, Quantum computation with quantum dots, Phys. Rev. A **57**, 120 (1998).

[7] G. Scappucci, C. Kloeffel, F. A. Zwanenburg, D. Loss, M. Myronov, J.-J. Zhang, S. De Franceschi, G. Katsaros, and M. Veldhorst, The germanium quantum information route, Nat. Rev. Mater. (2020).

[8] F. A. Zwanenburg, A. S. Dzurak, A. Morello, M. Y. Simmons, L. C. L. Hollenberg, G. Klimeck, S. Rogge, S. N. Coppersmith, and M. A. Eriksson, Silicon quantum electronics, Rev. Mod. Phys. **85**, 961 (2013).

[9] S. Nadj-Perge, V. S. Pribiag, J. W. G. Van den Berg, K. Zuo, S. R. Plissard, E. P. A. M. Bakkers, S. M. Frolov, and L. P. Kouwenhoven, Spectroscopy Of Spin-Orbit Quantum Bits In Indium Antimonide Nanowires, Phys. Rev. Lett. **108**, 166801 (2012).

[10] M. Karalic, C. Mittag, M. Hug, T. Tschirky, W. Wegscheider, K. Ensslin, T. Ihn, K. Shibata, and R. Winkler, Gate-tunable electronic transport in p-type GaSb quantum wells, Phys. Rev. B **99**, 115435 (2019).

[11] B. R. Bennett, R. Magno, J. B. Boos, W. Kruppa, and M. G. Ancona, Antimonide-based compound semiconductors for electronic devices: A review, Solid-State Electron. **49**, 1875 (2005).

[12] J. Sun, M. Peng, Y. Zhang, L. Zhang, R. Peng, C. Miao, D. Liu, M. Han, R. Feng, Y. Ma *et al.*, Ultrahigh hole mobility of Sn-catalyzed GaSb nanowires for high speed infrared photodetectors, Nano Lett. **19**, 5920 (2019).

[13] B. Ganjipour, M. Leijnse, L. Samuelson, H. Q. Xu, and C. Thelander, Transport studies of electron-hole and spin-orbit interaction in GaSb/InAsSb core-shell nanowire quantum dots, Phys. Rev. B **91**, 161301(R) (2015).

[14] B. Ganjipour, H. A. Nilsson, B. Mattias Borg, L.-E. Wernersson, L. Samuelson, H. Xu, and C. Thelander, GaSb nanowire single-hole transistor, Appl. Phys. Lett. **99**, 262104 (2011).

[15] C. Fasth, A. Fuhrer, M. T. Björk, and L. Samuelson, Tunable double quantum dots in InAs nanowires defined by local gate electrodes, Nano Lett. **5**, 1487 (2005).

[16] M. T. Björk, A. Fuhrer, A. E. Hansen, M. W. Larsson, L. E. Fröberg, and L. Samuelson, Tunable effective g factor in InAs nanowire quantum dots, Phys. Rev. B **72**, 201307(R) (2005).

[17] A. Fuhrer, L. E. Fröberg, J. N. Pedersen, M. W. Larsson, A. Wacker, M.-E. Pistol, and L. Samuelson, Few electron double quantum dots in InAs/InP nanowire heterostructures, Nano Lett. **7**, 243 (2007).

[18] M. Nilsson, L. Namazi, S. Lehmann, M. Leijnse, K. A. Dick, and C. Thelander, Single-electron transport in InAs nanowire quantum dots formed by crystal phase engineering, Phys. Rev. B **93**, 195422 (2016).

[19] D. Barker, S. Lehmann, L. Namazi, M. Nilsson, C. Thelander, K. A. Dick, and V. F. Maisi, Individually addressable double quantum dots formed with nanowire polytypes and identified by epitaxial markers, Appl. Phys. Lett. **114**, 183502 (2019).

[20] See Supplemental Material at http://link.aps.org/supplemental/10.1103/PhysRevB.103.L241411 for details on device fabrication and characterization, measurements on side-gated devices, and details of the fit in Fig. 4(d), which includes Refs. [12,43–47].

[21] F. Froning, M. Rehmann, J. Ridderbos, M. Brauns, F. Zwanenburg, A. Li, E. Bakkers, D. Zumbühl, and F. Braakman, Single, double, and triple quantum dots in Ge/Si nanowires, Appl. Phys. Lett. **113**, 073102 (2018).

[22] S. Dorsch, B. Dalelkhan, S. Fahlvik, and A. Burke, Side-gated, enhancement mode, InAs nanowire double quantum dot devices–Toward controlling transverse electric fields in spin-transport measurements, Nanotechnology **30**, 144002 (2019).

[23] J.-Y. Wang, G.-Y. Huang, S. Huang, J. Xue, D. Pan, J. Zhao, and H. Xu, Anisotropic pauli spin-blockade effect and spin–orbit interaction field in an InAs nanowire double quantum dot, Nano Lett. **18**, 4741 (2018).

[24] Y. Hu, H. O. Churchill, D. J. Reilly, J. Xiang, C. M. Lieber, and C. M. Marcus, A Ge/Si heterostructure nanowire-based double

quantum dot with integrated charge sensor, Nat. Nanotechnol. **2**, 622 (2007).

[25] F. Zwanenburg, A. Van Loon, G. Steele, C. Van Rijmenam, T. Balder, Y. Fang, C. M. Lieber, and L. Kouwenhoven, Ultrasmall silicon quantum dots, J. Appl. Phys. **105**, 124314 (2009).

[26] A. J. Keller, J. S. Lim, D. Sánchez, R. López, S. Amasha, J. A. Katine, H. Shtrikman, and D. Goldhaber-Gordon, Cotunneling Drag Effect In Coulomb-Coupled Quantum Dots, Phys. Rev. Lett. **117**, 066602 (2016).

[27] H. Thierschmann, R. Sánchez, B. Sothmann, F. Arnold, C. Heyn, W. Hansen, H. Buhmann, and L. W. Molenkamp, Three-terminal energy harvester with coupled quantum dots, Nat. Nanotechnol. **10**, 854 (2015).

[28] H. Bohuslavskyi, F. Ansaloni, A. Chatterjee, F. Fedele, T. Rasmussen, B. Brovang, J. Li, L. Hutin, B. Venitucci, B. Bertrand, M. Vinet, Y.-M. Niquet, and F. Kuemmeth, Reflectometry of charge transitions in a silicon quadruple dot, arXiv:2012.04791.

[29] W. G. Van der Wiel, S. De Franceschi, J. M. Elzerman, T. Fujisawa, S. Tarucha, and L. P. Kouwenhoven, Electron transport through double quantum dots, Rev. Mod. Phys. **75**, 1 (2002).

[30] D. Csontos and U. Zülicke, Large variations in the hole spin splitting of quantum-wire subband edges, Phys. Rev. B **76**, 073313 (2007).

[31] D. Csontos and U. Zülicke, Tailoring hole spin splitting and polarization in nanowires, Appl. Phys. Lett. **92**, 023108 (2008).

[32] D. Csontos, U. Zülicke, P. Brusheim, and H. Q. Xu, Lande-like formula for the g factors of hole-nanowire subband edges, Phys. Rev. B **78**, 033307 (2008).

[33] V. N. Golovach, A. Khaetskii, and D. Loss, Spin relaxation at the singlet-triplet crossing in a quantum dot, Phys. Rev. B **77**, 045328 (2008).

[34] C. Fasth, A. Fuhrer, L. Samuelson, V. N. Golovach, and D. Loss, Direct Measurement of the Spin-Orbit Interaction in a Two-Electron InAs Nanowire Quantum Dot, Phys. Rev. Lett. **98**, 266801 (2007).

[35] A. Pfund, I. Shorubalko, K. Ensslin, and R. Leturcq, Spin-state mixing in InAs double quantum dots, Phys. Rev. B **76**, 161308(R) (2007).

[36] H. A. Nilsson, P. Caroff, C. Thelander, M. Larsson, J. B. Wagner, L.-E. Wernersson, L. Samuelson, and H. Xu, Giant, level-dependent g factors in InSb nanowire quantum dots, Nano Lett. **9**, 3151 (2009).

[37] I. Van Weperen, B. Tarasinski, D. Eeltink, V. S. Pribiag, S. R. Plissard, E. P. A. M. Bakkers, L. P. Kouwenhoven, and M. Wimmer, Spin-orbit interaction in InSb nanowires, Phys. Rev. B **91**, 201413(R) (2015).

[38] F. A. Zwanenburg, C. E. van Rijmenam, Y. Fang, C. M. Lieber, and L. P. Kouwenhoven, Spin states of the first four holes in a silicon nanowire quantum dot, Nano Lett. **9**, 1071 (2009).

[39] M. Brauns, J. Ridderbos, A. Li, E. P. A. M. Bakkers, and F. A. Zwanenburg, Electric-field dependent g-factor anisotropy in Ge-Si core-shell nanowire quantum dots, Phys. Rev. B **93**, 121408(R) (2016).

[40] X.-J. Hao, T. Tu, G. Cao, C. Zhou, H.-O. Li, G.-C. Guo, W. Y. Fung, Z. Ji, G.-P. Guo, and W. Lu, Strong and tunable spin-orbit coupling of one-dimensional holes in Ge/Si core/shell nanowires, Nano Lett. **10**, 2956 (2010).

[41] A. P. Higginbotham, F. Kuemmeth, T. W. Larsen, M. Fitzpatrick, J. Yao, H. Yan, C. M. Lieber, and C. M. Marcus, Antilocalization of Coulomb Blockade in a Ge/Si Nanowire, Phys. Rev. Lett. **112**, 216806 (2014).

[42] Z. Wang, E. Marcellina, A. R. Hamilton, J. H. Cullen, S. Rogge, J. Salfi, and D. Culcer, Optimal operation points for ultrafast, highly coherent Ge hole spin-orbit qubits, npj Quantum Inf. **7**, 1 (2021).

[43] A. R. Wagner and S. W. Ellis, Vapor-liquid-solid mechanism of single crystal growth, Appl. Phys. Lett. **4**, 89 (1964).

[44] M. H. Magnusson, K. Deppert, J.-O. Malm, J.-O. Bovin, and L. Samuelson, Size-selected gold nanoparticles by aerosol technology, Nanostruct. Mater. **12**, 45 (1999).

[45] O. Wunnicke, Gate capacitance of back-gated nanowire field-effect transistors, Appl. Phys. Lett. **89**, 083102 (2006).

[46] B. Ganjipour, S. Sepehri, A. W. Dey, O. Tizno, B. M. Borg, K. A. Dick, L. Samuelson, L.-E. Wernersson, and C. Thelander, Electrical properties of GaSb/InAsSb core/shell nanowires, Nanotechnology **25**, 425201 (2014).

[47] A. S. Babadi, J. Svensson, E. Lind, and L.-E. Wernersson, Impact of doping and diameter on the electrical properties of GaSb nanowires, Appl. Phys. Lett. **110**, 053502 (2017).

Correction: The copyright license statement was presented incorrectly and has been fixed.